Available online at www.sciencedirect.com
ScienceDirect
Trans. Nonferrous Met. Soc. China 21(2011) 1367−1372
Transactions of Nonferrous Metals Society of China
www.tnmsc.cn

Solution of rectangular bar forging with bulging of sides by strain rate vector inner-product

WANG Lei[1], JIN Wen-zhong[2], ZHAO De-wen[3], LIU Xiang-hua[3]

1. School of Materials Science and Engineering, Shanghai University, Shanghai 200072, China;
2. Shanghai Shenhua Acoustics Equipment Co. Ltd., Shanghai 201709, China;
3. State Key Laboratory of Rolling and Automation, Northeastern University, Shenyang 110004, China

Received 19 July 2010; accepted 17 November 2010

Abstract: A new linear integration solution was constructed for determining the total pressure developed during forging of a rectangular bar with flat tools. The effective strain rate for rectangular bar forging with bulging was expressed in terms of four-dimensional strain rate vector. The inner-product of the vector was termwise integrated and summed. The integral mean value theorem was applied to determining the ratio of the strain rate components and the values of direction cosine of the vector and then an analytical solution of stress effective factor was obtained. The compression experiments of pure lead bar were performed to test the accuracy of the solution. The optimized results of total pressure by golden section search were compared with those of the indicator readings of the testing machine. It indicates that the optimized total pressures are 2.60%−10.14% higher than those measured. The solution is available and still an upper-bound solution.

Key words: rectangular bar forging; bulging; strain rate vector; inner-product; golden section search

1 Introduction

Forging a bar with flat tools is one of the simplest and most widely used processes in industry. However, its analysis is far from being simple. Hence a few approximate solutions have come forth, such as the upper bound [1−2], the lower bound [3−4] and slip line [5]. With the development of computers, numerical methods have been used to simulate the forging process [6−7]. ZHANG and XIE [8] and KANG et al [9] simulated forging process by FEM. GRASS et al [10] and GAO et al [11] used 3D-FEM simulation. And UBET has been successfully applied to solving the forging process by the authors [12−13]. These methods can all be applied to solving the forging, but just the numeric results are obtained.

In this work, the method so called inner-product of strain rate vector [14−15] is constructed and first applied to solving the bar forging and the analytic result of stress effective factor is obtained.

2 Velocity field

The origin of Cartesian coordinates is taken as the geometric centre of the body. The axes X, Y and Z divide the deforming zone into eight identical regions. So only the eighth is considered (Fig. 1). For any point with coordinates x, y and z, the velocity field is given by [1]

$$\boldsymbol{v} = v_x\boldsymbol{i} + v_y\boldsymbol{j} + v_z\boldsymbol{k} \tag{1}$$

$$v_x = \frac{v_0 x}{h} - 2A\frac{v_0}{h}\frac{l}{\pi}\sin\frac{\pi x}{2l},\quad v_y = A\frac{v_0}{h}y\cos\frac{\pi x}{2l},$$

$$v_z = -\frac{v_0}{h}z \tag{2}$$

where v_x, v_y, v_z are components of particle velocity in Cartesian coordinate system; v_0 is velocity of the top die; A is a constant to be determined by optimization on energy dissipation.

Foundation item: Project (51074052) supported by the National Natural Science Foundation of China; Project (20100470676) supported by the China Postdoctoral Science Foundation
Corresponding author: ZHAO De-wen; Tel: +86-24-83686423; E-mail: zhaodw@ral.neu.edu.cn
DOI: 10.1016/S1003-6326(11)60867-4

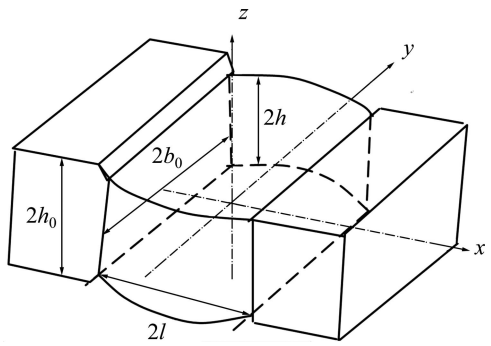

Fig. 1 Rectangular bar subjected to compression

The velocity field satisfies the boundary conditions: at $x=0$, $v_y = A\frac{v_0}{h}y$; at $x=l$, $v_y=0$. and the incompressibility condition, i.e.

$$\mathrm{div}\boldsymbol{v} = \frac{\partial v_x}{\partial x}+\frac{\partial v_y}{\partial y}+\frac{\partial v_z}{\partial z} = \dot{\varepsilon}_x+\dot{\varepsilon}_y+\dot{\varepsilon}_z = 0 \tag{3}$$

where

$$\dot{\varepsilon}_x = \frac{v_0}{h}-\frac{Av_0}{h}\cos\frac{\pi x}{2l},\quad \dot{\varepsilon}_y = \frac{Av_0}{h}\cos\frac{\pi x}{2l},$$

$$\dot{\varepsilon}_z = -\frac{v_0}{h},\quad \dot{\varepsilon}_{xy} = -\frac{\pi Av_0}{4lh}y\sin\frac{\pi x}{2l},$$

$$\dot{\varepsilon}_{xz} = \dot{\varepsilon}_{zx} = \dot{\varepsilon}_{yz} = \dot{\varepsilon}_{zy} = 0 \tag{4}$$

where $\dot{\varepsilon}_{ij}$ is the component of strain rate tensor.

From the mean value theorem of integral and Eq.(4), mean values of the strain rate can be obtained as follows:

$$\begin{aligned}\bar{\dot{\varepsilon}}_x &= \frac{1}{b_0 l}\int_0^{b_0}\int_0^{l}\dot{\varepsilon}_x\mathrm{d}x\mathrm{d}y\\ &= \frac{1}{b_0 l}\int_0^{b_0}\int_0^{l}\left(\frac{v_0}{h}-\frac{Av_0}{h}\cos\frac{\pi x}{2l}\right)\mathrm{d}x\mathrm{d}y\\ &= \frac{v_0}{h}-\frac{2Av_0}{\pi h},\\ \bar{\dot{\varepsilon}}_y &= \frac{2Av_0}{\pi h},\\ \bar{\dot{\varepsilon}}_z &= \dot{\varepsilon}_z,\\ \bar{\dot{\varepsilon}}_{xy} &= \frac{1}{b_0 l}\int_0^{l}\int_0^{b_0}\dot{\varepsilon}_{xy}\mathrm{d}x\mathrm{d}y = -\frac{Ab_0v_0}{4lh}\end{aligned} \tag{5}$$

It can be seen that Eq. (5) still satisfies

$$\dot{\varepsilon}_{ii} = \bar{\dot{\varepsilon}}_{ii} = 0$$

With the help of Eq. (2), the ratio of mean velocity can also be calculated as

$$\bar{v}_x = \frac{1}{l}\int_0^{l}v_x\mathrm{d}x = \frac{lv_0}{2h}-\frac{4Alv_0}{\pi^2 h},\quad \bar{v}_y = \frac{Ab_0v_0}{\pi h},$$

$$\frac{\bar{v}_y}{\bar{v}_x} = \frac{2\pi Ab}{\pi^2 l-8Al} \tag{6}$$

3 Total power

3.1 Internal deformation power

The integrand of plastic power is expressed by

$$\begin{aligned}N_{\mathrm{d}} &= \int_V \bar{\sigma}\bar{\dot{\varepsilon}}\mathrm{d}V\\ &= \sqrt{\frac{2}{3}}\sigma_{\mathrm{s}}\int_0^{b_0}\int_0^{l}\sqrt{\dot{\varepsilon}_x^2+\dot{\varepsilon}_y^2+\dot{\varepsilon}_z^2+2\dot{\varepsilon}_{xy}^2}\,h\mathrm{d}x\mathrm{d}y\\ &= \sqrt{\frac{2}{3}}\sigma_{\mathrm{s}}h\int_0^{b_0}\int_0^{l}\frac{\dot{\varepsilon}_x^2+\dot{\varepsilon}_y^2+\dot{\varepsilon}_z^2+2\dot{\varepsilon}_{xy}^2}{\sqrt{\dot{\varepsilon}_x^2+\dot{\varepsilon}_y^2+\dot{\varepsilon}_z^2+2\dot{\varepsilon}_{xy}^2}}\mathrm{d}x\mathrm{d}y\\ &= \sqrt{\frac{2}{3}}\sigma_{\mathrm{s}}h\cdot\\ &\quad\left\{\int_0^{b_0}\int_0^{l}\frac{\dot{\varepsilon}_x\mathrm{d}x\mathrm{d}y}{\sqrt{1+\left(\frac{\dot{\varepsilon}_y}{\dot{\varepsilon}_x}\right)^2+\left(\frac{\dot{\varepsilon}_z}{\dot{\varepsilon}_x}\right)^2+2\left(\frac{\dot{\varepsilon}_{xy}}{\dot{\varepsilon}_x}\right)^2}}+\right.\\ &\quad\int_0^{b_0}\int_0^{l}\frac{\dot{\varepsilon}_y\mathrm{d}x\mathrm{d}y}{\sqrt{1+\left(\frac{\dot{\varepsilon}_x}{\dot{\varepsilon}_y}\right)^2+\left(\frac{\dot{\varepsilon}_z}{\dot{\varepsilon}_y}\right)^2+2\left(\frac{\dot{\varepsilon}_{xy}}{\dot{\varepsilon}_y}\right)^2}}+\\ &\quad\int_0^{b_0}\int_0^{l}\frac{\dot{\varepsilon}_z\mathrm{d}x\mathrm{d}y}{\sqrt{1+\left(\frac{\dot{\varepsilon}_x}{\dot{\varepsilon}_z}\right)^2+\left(\frac{\dot{\varepsilon}_y}{\dot{\varepsilon}_z}\right)^2+2\left(\frac{\dot{\varepsilon}_{xy}}{\dot{\varepsilon}_z}\right)^2}}+\\ &\quad\left.\int_0^{b_0}\int_0^{l}\frac{2\dot{\varepsilon}_{xy}\mathrm{d}x\mathrm{d}y}{\sqrt{2+\left(\frac{\dot{\varepsilon}_x}{\dot{\varepsilon}_{xy}}\right)^2+\left(\frac{\dot{\varepsilon}_y}{\dot{\varepsilon}_{xy}}\right)^2+\left(\frac{\dot{\varepsilon}_z}{\dot{\varepsilon}_{xy}}\right)^2}}\right\}\\ &= \sqrt{\frac{2}{3}}\sigma_{\mathrm{s}}h\int_0^{b_0}\int_0^{l}\left(\dot{\varepsilon}_x l_1+\dot{\varepsilon}_y l_2+\dot{\varepsilon}_z l_3+2\dot{\varepsilon}_{xy}l_4\right)\mathrm{d}x\mathrm{d}y\\ &= \sqrt{\frac{2}{3}}\sigma_{\mathrm{s}}h\int_0^{b_0}\int_0^{l}\dot{\boldsymbol{\varepsilon}}\cdot\dot{\boldsymbol{\varepsilon}}^0\mathrm{d}x\mathrm{d}y\\ &= \sqrt{\frac{2}{3}}\sigma_{\mathrm{s}}h\left[\int_0^{b_0}\int_0^{l}\dot{\varepsilon}_x l_1\mathrm{d}x\mathrm{d}y+\int_0^{b_0}\int_0^{l}\dot{\varepsilon}_y l_2\mathrm{d}x\mathrm{d}y+\right.\\ &\quad\left.\int_0^{b_0}\int_0^{l}\dot{\varepsilon}_z l_3\mathrm{d}x\mathrm{d}y+2\int_0^{b_0}\int_0^{l}\dot{\varepsilon}_{xy}l_4\mathrm{d}x\mathrm{d}y\right]\\ &= \sqrt{\frac{2}{3}}\sigma_{\mathrm{s}}h\left(I_1+I_2+I_3+I_4\right)\end{aligned} \tag{7}$$

where $\dot{\boldsymbol{\varepsilon}} = \dot{\varepsilon}_x\boldsymbol{e}_1+\dot{\varepsilon}_y\boldsymbol{e}_2+\dot{\varepsilon}_z\boldsymbol{e}_3+2\dot{\varepsilon}_{xy}\boldsymbol{e}_4$ is strain rate vector; $\dot{\boldsymbol{\varepsilon}}^0 = l_1\boldsymbol{e}_1+l_2\boldsymbol{e}_2+l_3\boldsymbol{e}_3+l_4\boldsymbol{e}_4$ is unit vector; $l_i(i=1,2,3,4)$ is direction cosines of unit vector; and $I_i(i=1,2,3,4)$ is termwise integration of the strain rate vector.

From Eq. (7), the direction cosines are

$$\begin{cases} l_1=\left[1+\left(\dfrac{\dot\varepsilon_y}{\dot\varepsilon_x}\right)^2+\left(\dfrac{\dot\varepsilon_z}{\dot\varepsilon_x}\right)^2+2\left(\dfrac{\dot\varepsilon_{xy}}{\dot\varepsilon_x}\right)^2\right]^{-1/2} \\ l_2=\left[1+\left(\dfrac{\dot\varepsilon_x}{\dot\varepsilon_y}\right)^2+\left(\dfrac{\dot\varepsilon_z}{\dot\varepsilon_y}\right)^2+2\left(\dfrac{\dot\varepsilon_{xy}}{\dot\varepsilon_y}\right)^2\right]^{-1/2} \\ l_3=\left[1+\left(\dfrac{\dot\varepsilon_x}{\dot\varepsilon_z}\right)^2+\left(\dfrac{\dot\varepsilon_y}{\dot\varepsilon_z}\right)^2+2\left(\dfrac{\dot\varepsilon_{xy}}{\dot\varepsilon_z}\right)^2\right]^{-1/2} \\ l_4=\left[2+\left(\dfrac{\dot\varepsilon_x}{\dot\varepsilon_{xy}}\right)^2+\left(\dfrac{\dot\varepsilon_y}{\dot\varepsilon_{xy}}\right)^2+\left(\dfrac{\dot\varepsilon_z}{\dot\varepsilon_{xy}}\right)^2\right]^{-1/2} \end{cases} \tag{8}$$

The first termwise integration of strain rate vector inner product I_1 is

$$I_1=\int_0^{b_0}\int_0^{l}\dot\varepsilon_x l_1\mathrm{d}x\mathrm{d}y$$

$$=\int_0^{b_0}\int_0^{l}\dot\varepsilon_x\left[1+\left(\frac{\dot\varepsilon_y}{\dot\varepsilon_x}\right)^2+\left(\frac{\dot\varepsilon_z}{\dot\varepsilon_x}\right)^2+2\left(\frac{\dot\varepsilon_{xy}}{\dot\varepsilon_x}\right)^2\right]^{-1/2}\mathrm{d}x\mathrm{d}y$$

$$\approx\int_0^{b_0}\int_0^{l}\dot\varepsilon_x\left[1+\left(\frac{\bar{\dot\varepsilon}_y}{\bar{\dot\varepsilon}_x}\right)^2+\left(\frac{\bar{\dot\varepsilon}_z}{\bar{\dot\varepsilon}_x}\right)^2+2\left(\frac{\bar{\dot\varepsilon}_{xy}}{\bar{\dot\varepsilon}_x}\right)^2\right]^{-1/2}\mathrm{d}x\mathrm{d}y$$

Substituting Eqs. (4) and (5) into above integral, it follows that

$$I_1=\frac{\int_0^{b_0}\int_0^{l}\left(\dfrac{v_0}{h}-\dfrac{Av_0}{h}\cos\dfrac{\pi x}{2l}\right)\mathrm{d}x\mathrm{d}y}{\sqrt{1+\left(\dfrac{2A}{\pi-2A}\right)^2+\left(\dfrac{-\pi}{\pi-2A}\right)^2+2\left(\dfrac{-\pi Ab_0}{4l(\pi-2A)}\right)^2}}$$

$$=\frac{\dfrac{b_0l^2v_0}{h}\left(\dfrac{4A^2}{\pi}-4A+\pi\right)}{\sqrt{l^2(\pi-2A)^2+4A^2l^2+\pi^2l^2+\dfrac{1}{8}(\pi Ab_0)^2}}$$

With the same procedure, the other termwise integration results are

$$I_2=\frac{\dfrac{4A^2b_0l^2v_0}{\pi h}}{\sqrt{4A^2l^2+l^2(\pi-2A)^2+\pi^2l^2+\dfrac{1}{8}(\pi Ab_0)^2}}$$

$$I_3=\frac{-\dfrac{v_0}{h}\pi b_0l^2}{\sqrt{\pi^2l^2+l^2(\pi-2A)^2+4A^2l^2+\dfrac{1}{8}(\pi Ab_0)^2}}$$

$$I_4=\frac{-\dfrac{\pi A^2{b_0}^3v_0}{8h}}{\sqrt{\dfrac{1}{8}(\pi Ab_0)^2+l^2(\pi-2A)^2+4A^2l^2+\pi^2l^2}}$$

Substituting the results of I_1, I_2, I_3 and I_4 into Eq. (7) and rearranging yields

$$N_{\mathrm{d}}=\sqrt{\frac{2}{3}}\frac{\sigma_{\mathrm{s}}b_0v_0}{\pi}\cdot\sqrt{l^2(\pi-2A)^2+4A^2l^2+\pi^2l^2+\frac{\pi^2A^2{b_0}^2}{8}} \tag{9}$$

3.2 Friction power

Let $\tau_f=mk=\dfrac{m\sigma_s}{\sqrt{3}}$, $\left|\Delta v_f\right|=v_f=\sqrt{v_x^2+v_y^2}$, the friction power is

$$N_f=\int_s\tau_f\left|\Delta v_f\right|\mathrm{d}s=\frac{m\sigma_{\mathrm{s}}}{\sqrt{3}}\int_0^{b_0}\int_0^{l}\sqrt{{v_x}^2+{v_y}^2}\,\mathrm{d}x\mathrm{d}y$$

$$=\frac{m\sigma_{\mathrm{s}}}{\sqrt{3}}\int_0^{b_0}\int_0^{l}v_x\sqrt{1+\left(\frac{v_y}{v_x}\right)^2}\,\mathrm{d}x\mathrm{d}y$$

where τ_f is the shear along surface of velocity discontinuity; k is von Mises' constant of yield criterion; σ_{s} is effective flow stress; $\left|\Delta v_f\right|$ is the velocity discontinuity.

Substituting $\bar v_y/\bar v_x$ of Eq. (6) for v_y/v_x in above integrand, and integrating leads to

$$N_{\mathrm{f}}=\frac{m\sigma_{\mathrm{s}}b_0lv_0}{2\sqrt{3}\pi^2}\sqrt{\left(\pi^2-8A\right)^2\frac{l^2}{h^2}+4\pi^2A^2\frac{b_0^2}{h^2}} \tag{10}$$

3.3 Shear power

From Eq. (2), the velocity discontinuity at interface between deformation and external zones can be written as

$$\left|\Delta v_{\mathrm{z}}\right|=\left|\bar v_z\right|=\frac{1}{b_0h}\int_0^{h}\int_0^{b_0}\left|v_z\right|\mathrm{d}z\mathrm{d}y=\frac{v_0}{2}$$

So shear power becomes

$$N_{\mathrm{s}}=\int_s k\left|\Delta v_t\right|\mathrm{d}z\mathrm{d}y=\frac{kb_0hv_0}{2} \tag{11}$$

3.4 Stress effective factor and minimization

Let applied power $\bar pb_0lv_0=N_d+N_f+N_s$, and substitute Eqs. (9), (10) and (11) into it, then rearranging leads to

$$n_\sigma=\frac{\bar p}{\sigma_{\mathrm{s}}}=\sqrt{\frac{2}{3}}\sqrt{2-\frac{4A}{\pi}+\frac{8A^2}{\pi^2}+\frac{A^2}{8}\frac{{b_0}^2}{l^2}}+\frac{m}{2\sqrt{3}\pi}\sqrt{\left(\pi-\frac{8A}{\pi}\right)^2\frac{l^2}{h^2}+4A^2\frac{b_0^2}{h^2}}+\frac{h}{2\sqrt{3}l} \tag{12}$$

where n_σ is stress effective factor.

It is obviously that the stress effective factor n_σ is a function of A, m, b_0/h and l/h, also is a analytical solution. The optimum values of A and n_σ by the golden section search are shown in Fig. 2.

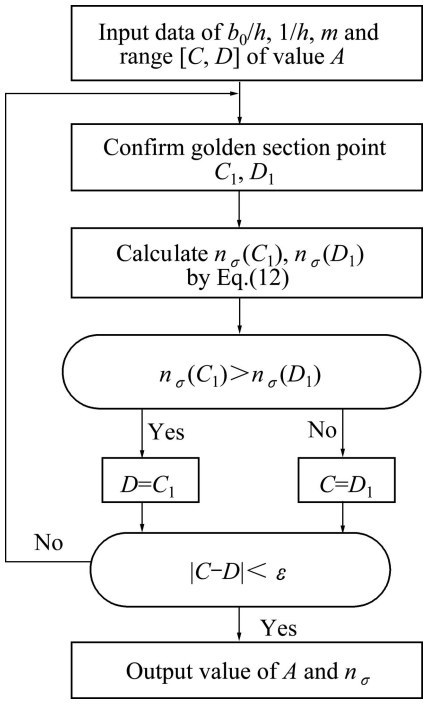

Fig. 2 Flow chart of golden section search

4 Experiment

In order to validate the solution in this work, the compression test was performed on 200 kN universal material testing machine. The dimensions of the three groups of pure lead specimens and the indicator readings of the machine during compressing are listed in Table 1. The ram speed was 30 mm/min.

Table 1 Specimen dimension and measured force

No.	$2b_0$/mm	$2h_0$/mm	$2l$/mm	$2b_1$/mm	$2h$/mm	F_m/kN
1	20.33	20.33	30.0	21.70	18.50	14.10
2	39.86	19.70	30.0	42.16	17.49	30.00
3	39.97	10.12	15.0	40.75	9.08	14.50

Taking No.1 specimen as an example, the calculating procedure is given in detail as follows.

From Table 1, l/h=1.62, b_0/h=1.10, and m=0.2 (for quenched steel and lapped face). Then inputting the values of l/h, b_0/h, and m into Eq. (12) and optimizing by flow chart in Fig. 2, the optimum result becomes: A=0.78, n_σ=1.22.

From Table 1, the strain and the strain rate for No.1 specimen are $\varepsilon=\ln\dfrac{20.33}{18.50}=0.094$; $\dot{\varepsilon}=\dfrac{\varepsilon}{t}=\dfrac{30/60}{20.33-18.50}\ln\dfrac{20.33}{18.50}=0.026\ \ \mathrm{s}^{-1}$.

According to the values of ε and $\dot{\varepsilon}$, the yield stress for pure lead is σ_s=20.05 MPa [16]. Then the total compression force for No.1 sample is

$$F_0=n_\sigma\sigma_s\frac{2l(2b_1+2b_0)}{2\times1\ 000}=15.48\ \ \mathrm{kN}$$

Comparing it with the measured value F_m in Table 1, the relative error can (E) be expressed as

$$E=\frac{15.48-14.10}{14.10}\times100\%=9.79\%$$

With the same procedure, the optimized results of No. 2 and 3 specimens can also be obtained and listed in Table 2.

Table 2 Optimized results for three groups of specimens

No.	l/h	b_0/h	A	n_σ	F_0/kN	E/%
1	1.62	1.10	0.78	1.22	15.48	9.79
2	1.72	2.28	0.61	1.25	30.78	2.60
3	1.65	4.40	0.34	1.32	15.97	10.14

From the results we can know that the relative errors between the optimized results and the measured ones are from 2.60% to 10.14%, all admitted in engineering.

5 Discussion

In order to examine the characteristics of the present solution, the optimum values of A and n_σ were optimized for the values of l/h varying from 0.5 to 5.5 and b_0/h equal to 1.10, 2.28 and 4.40 and m from 0.2 to 1.0. The value of parameter A signifies the extent of bulging. From Fig. 3 it can be seen that bulging parameter A increases with increasing l/h or decreasing b_0/h for a given m. Figure 4 shows that n_σ increases as m increases for given values of b_0/h and l/h, but always exists a minimum value of n_σ in each curve.

Fig. 5 shows that the value of n_σ increases with increasing b_0/h and m for a given l/h.

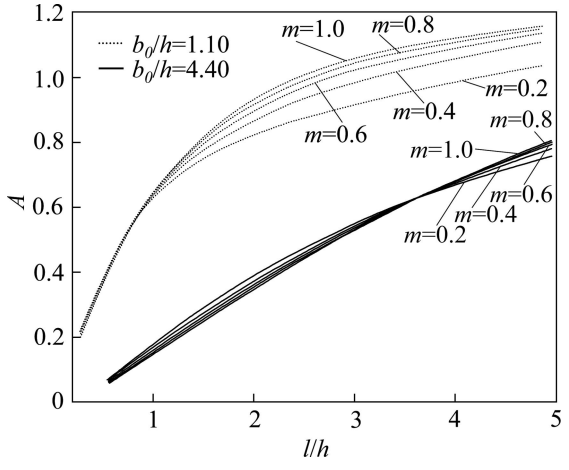

Fig. 3 Influence of l/h and b_0/h on optimum values of A

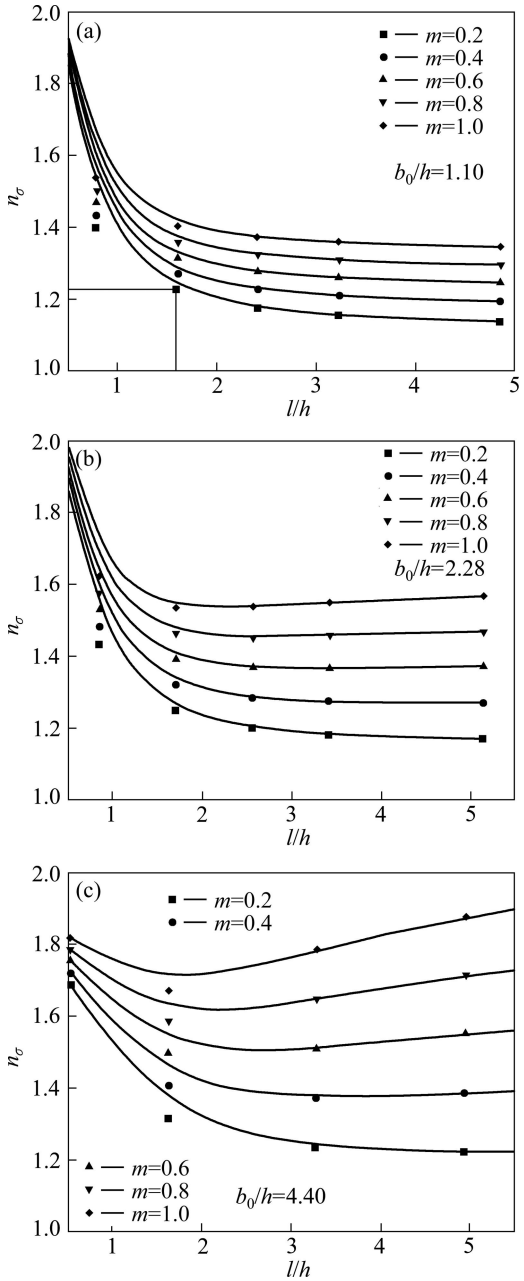

Fig. 4 Influence of l/h, b_0/h and m on n_σ for optimum values of A

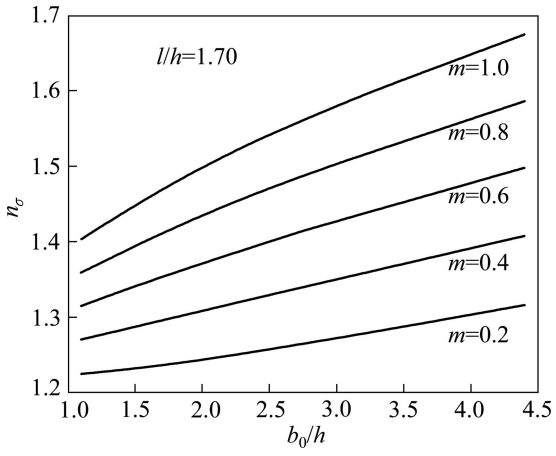

Fig. 5 Influence of b_0/h on n_σ for given l/h

6 Conclusions

1) With the help of strain rate vector inner-product, the analytical solution of stress effective factor n_σ for rectangular bar forging is obtained. And n_σ is a function of A, m, b_0/h and l/h.

2) Through pure lead compression test, the optimized results by above solution are 2.60%−10.14% higher than those measured.

3) The relationship among A, l/h, b_0/h and m can be described. Bulging parameter A increases with increasing l/h or decreasing b_0/h for a given m.

References

[1] SAGAR R, JUNEJA B L. An upper bound solution for flat tool forging taking into account the bulging of sides [J]. International Journal of Machine Tool Design and Research, 1979, 19(4): 253−258.

[2] WANG Zhen-fan. Upper bound solution and its application in metal forming [M]. Shenyang: Northeast University of Technology Press, 1991: 200−203. (in Chinese)

[3] HASHMI M S J. A lower bound solution for the plane strain extrusion forging process [J]. Mathematical and Computer Modelling, 1988, 11: 1183−1188.

[4] SINGH D N, BASUDHAR P K. Optimal lower-bound solutions of plane-strain metal indentation and extrusion problems [J]. Journal of Materials Processing Technology, 1995, 49(1−2): 75−84.

[5] SAMOLYK G, PATER Z. Application of the slip-line field method to the analysis of die cavity filling [J]. Journal of Materials Processing Technology, 2004, 153−154: 729−735.

[6] KOPP R. Some current development trends in metal-forming technology [J]. Journal of Materials Processing Technology, 1996, 60(1−4): 1−9.

[7] PITTMAN J F T. Numerical analysis of forming processes [M]. New York: John Wiley and Sons, 1984: 32−33.

[8] ZHANG Zhi-hao, XIE Jian-xin. A numerical simulation of super-plastic die forging process for Zr-based bulk metallic glass spur gear [J]. Material Science and Engineering A, 2006, 433(1−2): 323−328.

[9] KANG G J, SONG W J, KIM J, KANG B S, PARK H J. Numerical approach to forging process of a gear with inner cam profile using FEM [J]. Journal of Material Processing Technology, 2005, 164−165: 1212−1217.

[10] GRASS H, KREMPASZKY C, WERNER E. 3-D FEM-simulation of hot forming processes for the production of a connecting rod [J]. Computational Materials Science, 2006, 36(4): 480−489.

[11] GAO Tao, YANG He, LIU Yu-li. Backward tracing simulation of precision forging process for blade based on 3D FEM [J]. Transactions of Nonferrous Metals Society of China, 2006, 36(S2): 639−644.

[12] HWANG B C, HONG S J, BAE W B. An UBET analysis of the non-axisymmetric extrusion/forging process [J]. Journal of Material Processing Technology, 2001, 111(1−3): 135−141.

[13] MOLLER J, TRAN L, SHRADER D, DOUGLAS J R, KUHLMAN G W. Augmented upper bound element technique for prediction of temperature and strain in forgings [J]. Journal of Material Processing Technology, 2004, 152(2): 162−175.

[14] ZHAO De-wen. Mathematical solutions of continuum forming force [M]. Shenyang: Northeastern University Press, 2003: 421−425. (in Chinese)

[15] ZHAO De-wen, JIN Wen-zhong, WANG Lei, LIU Xiang-hua. Inner-product of strain rate vector through direction cosine in coordinates for disk forging [J]. Transactions of Nonferrous Metals Society of China, 2006, 16(6): 1320−1324.

[16] LOIZOU N, SIMS R B. The yield stress of pure lead in compression [J]. Journal of the Mechanics and Physics of Solids, 1953: 1(4): 234−243.

应变矢量内积法求解带鼓形的矩形坯锻压

王 磊[1], 金文忠[2], 赵德文[3], 刘相华[3]

1. 上海大学 材料科学与工程学院，上海 200072；
2. 上海申华声学装备有限公司，上海 201709；
3. 东北大学 轧制技术及连轧自动化国家重点实验室，沈阳 110004

摘 要：提出一种新的线性化积分方法用于求解平锤头压缩带外端的矩形件。在锻压过程中，锤头没有覆盖整个工件，并且工件的侧面通过变形产生鼓形。应用该方法得到了平均锻压力，同时在求解的过程中进行了下列假设：工件与工具间的摩擦力为常数，工件是刚−塑性材料，锻压是在低速度下进行的。然后，通过纯铅的锻压实验，将由黄金分割法得到的优化结果与试验机的实测值进行比较，结果表明优化值比实测值高 2.60%−10.14%，这在工程上都是允许的。

关键词：矩形坯锻压；鼓形；应变速率矢量；内积；黄金分割法

(Edited by LI Xiang-qun)